

Applying CFD for Studying the Dynamic and Thermal Behavior of an Indirect Solar Dryer: Parametric Analysis

S. KHALDI
A. N. KORTI

*ETAP Laboratory, Department of Mechanics
University of Tlemcen, FT
BP 230, 13000 Tlemcen, Algeria
kha.souhila@live.fr
korti72@yahoo.fr*

S. ABBOUDI

*2 IRTES-M3M - EA 7274, University of Technology of Belfort-Montbéliard
Sévenans, 90010 Belfort Cedex, France
said.abboudi@utbm.fr*

Received (18 September 2017)

Revised (14 October 2017)

Accepted (18 November 2017)

In this work, an indirect solar dryer integrated thermal storage for drying figs. (*Ficus carica*) is studied numerically. Unsteady turbulent airflow and heat transfer through a two-dimensional model is carried out for a typical day of August under the climatic conditions of Tlemcen (Algeria). Effects of air inlet size and thickness of the packed bed on the dynamic and thermal behaviors of the dryer with and without packed bed have been discussed. The study shows that: (1) Increase the inlet size from 0.04 m to 0.10 m can accelerate the extraction of air by about 13% and reduce the maximum crops temperature by about 14%. (2) The packed bed can reduce the mass flow rate extracted by 22% and the fluctuations of air temperature by 1.3%. (3) A packed bed with a thickness of 0.15 m can extend the operating time of the dryer up to 23%.

Keywords: solar dryer, free convection, packed bed, CFD.

1. Introduction

The fig is a wealth, a symbol, in short a treasure of Algeria. Figs. are picked late summer until mid-September. During this season, the figs are eaten fresh. To perpetuate this gustatory pleasure all over the year, the farmers dry the figs. Figs are composed of nothing in greater amount than water which is denoted by moisture content. During the drying process, the product is exposed to a dry and hot airflow. When air temperature increased the capacity of air to hold water vapor increased

too. However, there is a limit on how much water vapor the air can hold at any given temperature. The air exchange rate is also factor causing evaporation because it carries away moist air which is replaced with dry air, thus increasing the rate of evaporation.

Solar drying is a fundamental option for preserving food. It is probably the first ever food preserving method used by man. Even today, most of the agricultural products are dried under the sun [1, 2]. The disadvantages of this method include larger drying period, loss of quality, and losses due to birds and rodents attack [3]. Solar dryers used for food and crop drying are very useful devices. It not only saves energy but also saves lot of time. A great deal of research has been done to improve the design and operation of solar dryers, which are generally classified into direct, indirect and mixed mode systems. The drying air can be moved on naturally by buoyancy (natural circulation) or by using a fan (forced circulation) [4].

Due to the solar intermittent, the solar air heater provides the hot air with a large variation in the temperature to the dryer. A storage unit is a key component to overcome such issue and improve the efficiency of solar systems [5, 6]. It is necessary to use thermal storage devices integrated in the solar dryer for continuous drying during off-sunshine hours. It is also included to reduce the fluctuation in outlet temperature of hot air.

Lalit M. et al. [7] summarized the past and recent researches in the field of thermal energy storage technology in materials as sensible and latent heat in solar dryers for drying of agricultural food products. They found that solar dryer incorporated a storage unit is very beneficial for the humans as well as for the energy conservation.

The main factor that affects the overall drying system efficiency is the airflow behavior. Predicting this behavior helps to optimize the whole drying system. To achieve that, it is necessary to have a good knowledge of the laws of heat and mass transfer. Several numerical studies available in the literature presented the thermodynamic modeling of the solar dryers, where they solved a state equation for each component of the solar dryer to determinate the temperature, mass flow rate and moisture content. This method is fast, but the effects of many parameters like geometric complexity are being neglected [8-10].

The most important component of the dryer is the cabinet of drying. Modeling this part of the dryer using the thermodynamic method is not sufficient for the creation of good quality solutions. Indeed, the flow in this area is completely two dimensional especially if the geometry is complicated. In this case the use of computational fluid dynamics (CFD) codes is a convenient way to evaluate the airflow parameters. This method helps to predict which design changes are most crucial to enhance performance. Several studies used this method. [11-13]. Wei C. et al. [14] analyzed the heat and mass transfer through a natural draying chamber coupled with a chimney and porous absorber. They considered that the airflow is turbulence convection using $k-\varepsilon$ model. They studied the influences of the porous absorber and the height of dryer on the performance of heat transfer and airflow within the drying system. They found that the use of an inclined porous absorber increase the temperature and velocity at the outlet. The higher drying system leads to the lower airflow temperature and the higher airflow velocity at the chimney exit. Romero V.M. et al. [15] presented a numerical and experimental study of the vanilla drying process in an indirect solar dryer. In this paper, the authors used the CFD fluent

program to solve the governing equations. They found a good agreement between the numerical and experimental results at solar collector outlet. However, there is a difference between the results through the cabinet. This disagreement is due to have been considered a constant convection heat transfer coefficient in the ambient. Ghaffariet A. al. [16] presented a numerical study of a solar dryer using the CFD using a new approach for the modeling of the drying cabinet. They calculated the heat transferred during the drying process and incorporated this value as negative heat source in the trays, which are considered as a porous jump. As result, the authors found that the model was in good agreement with the experimental results in the literature, that reveals the porous jump modeling be appropriate for the entire simulation. Amanlou Y. et al. [17] analyzed a new design of drying cabinet. They studied seven different geometries of cabinet dryer using fluent software. The authors assumed the trays as a porous media for the airflow using empirical data. As results, they found that increasing the inlet size gives higher drying air temperature. Increasing the divergence angle improves the air velocity distribution and transferring the air exit location to the center causes a more uniform air velocity distribution at the tray zones. Shifting the air exit to the right of design would weaken air velocity distribution at the dryer chamber corners. Suhaimi M. et al. [18] presented two-dimensions simulation of a tray dryer system using CFD method. They try to get a uniform airflow distribution throughout the drying chamber by studying three different positions for trays and adding baffles into the drying chamber. They found that the position of trays effects the airflow distribution and the additional of baffle gives better result in term of uniform airflow distribution for each tray and shorter drying time.

Goyal R. K. et al. [19] have proposed a reverse flat plate absorber as air heater for drying application. They solved a state equation for each component of the solar dryer to analyze the thermal evolution of the solar dryer. They try to optimize the vent area of the dryer for speedy flow of humid air from the drying chamber to the atmosphere. They found that this dryer can be operated for longer and provide higher temperature than normal cabinet dryers, because of minimum bottom and top heat losses. To improve the performance of this solar dryer, Jain D. [20] proposed to add a packed bed as storage medium and a solar chimney to create an accelerated flow through the drying cabinet. He proposed mathematical model (global energy balance approach) based on the knowledge of heat and mass transfer coefficients between different components of the system. The study used the correlations to model the heat transfer of the airflow, which is assumed in forced convection. They found that the thermal storage is very pertinent in reducing the fluctuation of temperature and the proposed mathematical model is useful for evaluating the performance of the solar dryer.

In the present study, we propose to analyze the dynamic and thermal behavior of the solar dryer improved by Jain using the computational fluid dynamics (CFD).

2. Description of the solar dryer

The physical model is presented in Fig. 1. The dryer has total collector area of 1 m^2 . Reflector in a polygonal form with five flat segments of identical size reflects the solar radiation to the horizontal absorber-1 (aluminum) which is facing down. Absorber-

1 absorbs the reflected solar radiation and the heat is transferred by convection to the airflow. The drying installation is placed above the absorber-1 at a distance of $e = 0.04$ m. This space is necessary for entering ambient air. A packed bed with a porosity of 0.4 and a particle diameter of 0.023 m is placed before the two drying trays. The air heated by the absorber-1 flows towards the packed bed and warms up the gravel. After, it flows towards the crops trays and dries the figs.

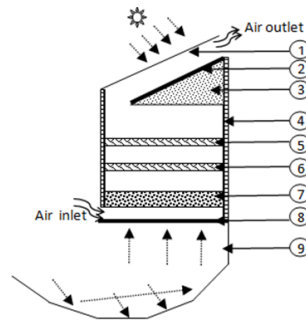


Figure 1

An inclined solar chimney (35°) is placed on top of the dryer; it is used to increase the velocity of drying air that enters the drying chamber. This chimney is composed of glass cover and absorber-2 (aluminum). A heat storage material (granite) is placed under absorber-2. In the other side, the absorber-2 absorbs solar irradiation transmitted through the glass cover. A part of this heat is transferred by convection to the airflow in channel; creating a difference in temperature between the chimney and the chamber. The other part is stored by the granite to be used during off-sunshine hours for holding the airflow during this period. The thermophysical properties of the different materials used in the solar dryer are presented at tables 1 and 2 [21, 22].

3. Mathematical modeling

3.1. Assumptions

To simplify the problem, the following assumptions were made:

1. The fluid is viscous and Newtonian.
2. The flow is turbulent, two dimensional and unsteady.
3. The boussinesq approximation is applied for the buoyancy.
4. The thermophysical properties of the air and solids are considered constants.
5. The packed bed is a homogeneous porous media.

3.2. Basic governing equations

This model is based on the conservation equations of fluid mechanics: the continuity the momentum and the energy equations. It is also takes into account the turbulent behavior. There are many turbulent models embedded in commercial codes for turbulent flows. Of all turbulence models available, the standard $k - \varepsilon$ model still remains an industrial standard and its successful applications are found in many studies [13, 23]. The general transport equations, which describe the thermal behavior of the dryer system, are summarized as follows:

3.2.1. Modeling Airflow

1. Continuity equation:

$$\frac{\partial \rho}{\partial t} + \frac{\partial (\rho u)}{\partial x} + \frac{\partial (\rho v)}{\partial y} = 0 \quad (1)$$

2. Momentum equation:

$$\frac{\partial (\rho u)}{\partial t} + \frac{\partial (\rho u u)}{\partial x} + \frac{\partial (\rho v u)}{\partial y} = \frac{\partial}{\partial x} \left(\mu \frac{\partial u}{\partial x} \right) + \frac{\partial}{\partial y} \left(\mu_t \frac{\partial u}{\partial y} \right) + S_u \quad (2)$$

$$\frac{\partial (\rho v)}{\partial t} + \frac{\partial (\rho u v)}{\partial x} + \frac{\partial (\rho v v)}{\partial y} = \frac{\partial}{\partial x} \left(\mu_t \frac{\partial v}{\partial x} \right) + \frac{\partial}{\partial y} \left(\mu_t \frac{\partial v}{\partial y} \right) + S_v \quad (3)$$

The source terms in momentum equation are expressed:

$$S_u = -\frac{\partial p}{\partial x} + \frac{\partial}{\partial x} \left(\mu_t \frac{\partial u}{\partial x} \right) + \frac{\partial}{\partial y} \left(\mu_t \frac{\partial v}{\partial y} \right) \quad (4)$$

$$S_v = -\frac{\partial p}{\partial y} + \frac{\partial}{\partial x} \left(\mu_t \frac{\partial u}{\partial y} \right) + \frac{\partial}{\partial y} \left(\mu_t \frac{\partial v}{\partial y} \right) + \rho g \beta (T - T_{ref}) \quad (5)$$

1. Energy equation:

$$\frac{\partial (\rho T)}{\partial y} + \frac{\partial (\rho u T)}{\partial x} + \frac{\partial (\rho v T)}{\partial y} = \frac{1}{\rho} \left(\frac{\mu}{Pr} + \frac{\mu_t}{\sigma_t} \right) \left(\frac{\partial^2 T}{\partial x^2} + \frac{\partial^2 T}{\partial y^2} \right) \quad (6)$$

2. Turbulence kinetic energy k equation:

$$\rho \left(\frac{\partial k}{\partial t} + \frac{\partial (k u)}{\partial x} + \frac{\partial (k v)}{\partial y} \right) = \left(\mu + \frac{\mu_t}{\sigma_k} \right) \left(\frac{\partial^2 k}{\partial x^2} + \frac{\partial^2 k}{\partial y^2} \right) + \rho G_k - \rho \varepsilon \quad (7)$$

3. Dissipation rate of turbulent kinetic ε equation:

$$\rho \left(\frac{\partial \varepsilon}{\partial t} + \frac{\partial (\varepsilon u)}{\partial x} + \frac{\partial (\varepsilon v)}{\partial y} \right) = \left(\mu + \frac{\mu_t}{\sigma_\varepsilon} \right) \left(\frac{\partial^2 \varepsilon}{\partial x^2} + \frac{\partial^2 \varepsilon}{\partial y^2} \right) + \frac{\varepsilon}{k} (c_1 \rho G_k - c_2 \rho \varepsilon) \quad (8)$$

where:

$$\mu_t = \frac{\rho c_\mu k^2}{\varepsilon} \quad \text{and} \quad G_k = \frac{\mu_t}{\rho} \frac{\partial u_i}{\partial x_j} \left\{ \frac{\partial u_i}{\partial x_j} + \frac{\partial u_j}{\partial x_i} \right\} \quad (9)$$

The turbulence model contains five constants which were assigned the following values: $c = 0.09$, $c_1 = 1.44$, $c_2 = 1.92$, $\sigma_k = 1$, $\sigma_\varepsilon = 1.3$; $\sigma_t = 1$

3.2.2. Modeling the porous bed

The flow in the porous medium is governed by the model of Brinkman-Forchheimer Extended Darcy:

1. Continuity equation

$$\frac{\partial \rho}{\partial t} + \frac{\partial (\rho u_f)}{\partial x} + \frac{\partial (\rho v_f)}{\partial y} = 0 \quad (10)$$

1. Momentum equation:

$$\begin{aligned} \rho \frac{\partial u_f}{\partial t} + \frac{\rho}{2} \left(u_f \frac{\partial u_f}{\partial x} + v_f \frac{\partial u_f}{\partial y} \right) &= -\frac{\partial p}{\partial x} \\ + \frac{\partial}{\partial x} \left(\mu_{eff} \frac{\partial u_f}{\partial x} \right) + \frac{\partial}{\partial y} \left(\mu_{eff} \frac{\partial u_f}{\partial y} \right) - \mu \frac{u_f}{\theta} + \frac{\rho C}{\sqrt{\theta}} |\vec{u}_f| u_f \end{aligned} \quad (11)$$

$$\begin{aligned} \rho \frac{\partial v_f}{\partial t} + \frac{\rho}{2} \left(u_f \frac{\partial v_f}{\partial x} + v_f \frac{\partial v_f}{\partial y} \right) &= -\frac{\partial p}{\partial x} + \frac{\partial}{\partial x} \left(\mu_{eff} \frac{\partial v_f}{\partial x} \right) \\ + \frac{\partial}{\partial y} \left(\mu_{eff} \frac{\partial v_f}{\partial y} \right) - \mu \frac{v_f}{\theta} + \frac{\rho C}{\sqrt{\theta}} |\vec{v}_f| v_f + \rho g \beta (T - T_{ref}) \end{aligned} \quad (12)$$

2. Energy equation:

$$(\rho c)_m \frac{\partial T}{\partial t} + (\rho c)_m \left(u_f \frac{\partial T}{\partial x} + v_f \frac{\partial T}{\partial y} \right) = K_m \frac{\partial}{\partial x} \left(\frac{\partial T}{\partial x} \right) + K_m \frac{\partial}{\partial y} \left(\frac{\partial T}{\partial y} \right) \quad (13)$$

where the thermo-physical parameters are calculated by the mixture method

$$(\rho c)_m = (\rho c)_f + (1 -)(\rho c)_s \quad \text{and} \quad K_m = K_f + (1 -)K_s \quad (14)$$

$$\theta = \frac{D_p^{23}}{150(1 -)^2}; \quad C = \frac{3.5(1 -)}{D_p^3} \quad (15)$$

θ is the permeability and C is the inertial resistance factor, its values equal to $6.29 \cdot 10^{-7} \text{ m}^2$ and 1719.4 m^{-1} , respectively.

3.2.3. Modeling of the crops tray

Fruit trays were assumed as porous media for airflow. It is modeled by the addition of a momentum source term (tS_i) to the standard fluid flow equations:

$$S_i = -C'_0 |v|^{C'_1} \quad (16)$$

The coefficients C'_0 , C'_1 and porosity are proposed for the figs fruit by Amanlou Y. et al. [17]. Its values are 0.029, 0.6849 and 50.61%, respectively.

3.2.4. Modeling of thin layer drying

For all models, the two-term exponential model demonstrated the best performance in fitting the experimental data [24].

$$MR = \frac{M(t) - Me}{M_0 - Me} = a \exp(-k_0 t) + b(-k_1 t) \quad (17)$$

a, b, k_0, k_1 are the analysis coefficients for the two-term exponential equation, its equal to 0.828370, 0.164038, 0.049360, 0.00435, respectively. The equilibrium moisture content Me of figs at different relative humidities and temperatures levels was calculated using the GAB equation [25]:

$$Me = \frac{M_m C' k' a_w}{(1 - k' a_w) [(1 - C') k' a_w]} \tag{18}$$

$$C' = 1.77 \exp\left(\frac{-1.55}{RT}\right) \tag{19}$$

$$k' = 0.05 \exp\left(\frac{25.2}{RT}\right) \tag{20}$$

$R = 8.314 \text{ J K}^{-1} \text{ mol}^{-1}$, $a_w = 0.4$.

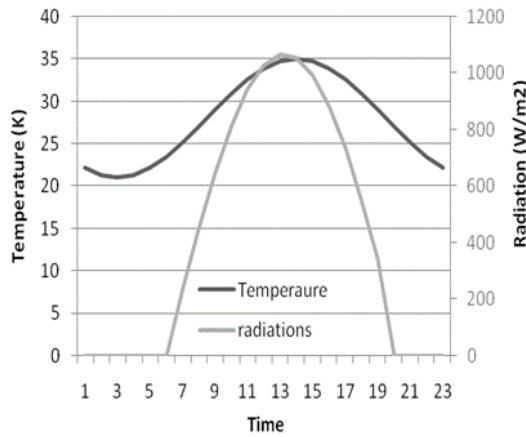


Figure 2

3.3. Initial and boundary conditions

Numerical simulations were performed for a typical day of August, under the climatic conditions of Tlemcen, Algeria. The solar irradiance variation [26] and the outside temperature (Météo Tlemcen Zenata) are presented in Fig. 2 and approximated by Eqs. (21) and (22) respectively:

$$T_a(t) = 28 + 7 \cos\left[\frac{\pi}{11}(t - 14)\right] \tag{21}$$

$$G_{sun} = 1068 \sin\left[\pi \frac{t - 6}{14.5}\right] \quad 6 < t < 19 \tag{22}$$

The dryer is only heated by direct sunlight from 06:00 to 19:00. The fluid in the solar dryer is initially stagnant and at a uniform temperature which is the same as the ambient temperature.

1. *Wooden Wall boundary conditions:* No slip conditions employed at inner side of the dryer chamber wall surface. At the exterior, the surfaces are exposed to the convection boundary condition:

$$-K_w \frac{dT}{dn} = h_0 (T_w - T_a) \quad u = 0 \quad v = 0 \quad (23)$$

Heat transfer coefficient is given by Watmuff J. H. et al. [27]

$$h_0 = 2.8 + 3V_w \quad (24)$$

where: V_w is the wind velocity taken equal to 3 m/s.

2. *The glass surface:* is exposed to no slip condition and combined external convection and radiation boundary conditions.

$$-K_g \frac{dT}{dn} = \alpha_g G_{sun}(t) + h_0 (T_g - T_a) + \varepsilon_g \sigma (T_g^4 - T_{sky}^4) \quad u = 0 \quad v = 0 \quad (25)$$

The sky temperature is given by Swinbank W.C. [28]:

$$T_{sky} = 0,0552 T_a^{1.5} \quad (26)$$

3. *The solar absorber surface-1:* is exposed to no slip condition and combined external convection and radiation boundary conditions:

$$-K_{a1} \frac{dT}{dy} = G_{sun}(t) \rho' A_t \alpha_{a1} + h_0 (T_{a1} - T_a) \quad u = 0 \quad tv = 0 \quad (27)$$

4. *The solar absorber surface-2:* is exposed to no slip condition and combined external convection and radiation boundary conditions.

$$-K_{a2} \frac{dT}{dn} = G_{sun}(t) \tau_g \alpha_{a2} \quad u = 0 \quad v = 0 \quad (28)$$

5. *Inlet boundary condition:* the uniform temperature and pressure is given at the inlet of the solar dryer.

$$T_{inlet} = T_a, p_{inlet} = 10^5 \text{Pa}$$

6. *Outlet boundary condition:* an outlet pressure is fixed.

$$p_{outlet} = 10^5 \text{Pa}$$

4. Results and discussion

The governing equations with the associated boundary and initial conditions are solved with finite volume method using Fluent Software 6.3 with additional subroutines incorporated (UDF's) for specifying unsteady state boundary conditions. The discretization of the equations is fully conservative and time implicit. The SIMPLE algorithm was used for pressure-velocity coupling. The convergence of solutions is assumed when the maximum normalized residue for all cells is less than 10^{-5} . A test analysis of the grid independence showed that the mesh grid (16,092) is good enough for the studied geometry. Several values of time step (between 10 and 70 s) have been examined for the chosen grid. Finally, Δt used in computations is 30 s.

4.1. Validation results

In order to validate the obtained results, a comparison with the experimental results performed by Jyotirmay M. et al. [29] is done. The authors presented an experimental and numerical study of the natural ventilation in a cavity similar to the dryer chamber. The cavity has a surface of 1 m^2 , an inlet opening and a roof solar chimney. In order to simulate the natural convection through this cavity, the CFD method is used and the airflow is considered as turbulence convection using $k-\varepsilon$ model. Fig. 3 illustrates the evolution of the measured and calculated temperature and velocity of airflow at the outlet of chimney with solar intensity.

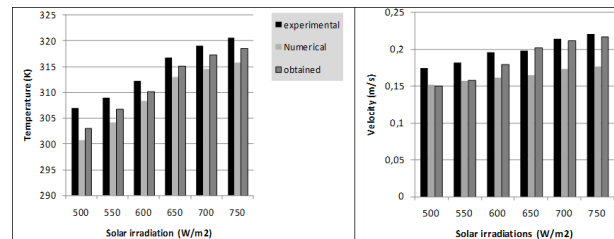


Figure 3

The obtained results are in a good agreement with those of the experimental results presented in reference [29]. The average relative error of 0.96% for the temperature and 14% for the velocity are observed. This concludes that our model allows simulating the dynamic and the thermal behavior correctly inside the solar dryer. It should be noticed that average relative error between the experimental and numerical results presented in reference [29] are 1.6 % and 16.8 % for the temperature and velocity, respectively. Then, the obtained results using the CFD approach are closer to the experimental compared to the global one used by the authors. This encourages us to analyze the performance of the solar dryer proposed by Jain D. [20] using the proposed CFD model.

4.2. Solar dryer without packed bed

4.2.1. Temperature evolution of different components

Fig. 4. shows the temperature evolution (at $x = 0.5$ m) of the different components (absorber-1 and 2, crops in tray-1 and 2, and outlet temperature) of the solar dryer with the time. During sunlight hours, the absorber-1 and 2 warm up by absorbing solar radiations. The temperature of the absorber-1 (T_{a1}) is higher than the absorber-2 (T_{a2}). The heat received by the absorber-1 is completely transmitted to the airflow coming from the outside. In contrast, the absorber-2 is in direct contact with granite, which absorbs and stores a part of the received heat. This leads to decrease the maximum temperature of T_{a2} (350 K) compared to T_{a1} (370 K). Then, T_{a1} decreases clearly faster than T_{a2} because the granite releases its heat stored. During the first half day, the crops temperature of the two trays increased and achieved 319 K and 322 K as maximum for tray-1 and tray- 2 respectively, and decreased after that to 295 K for the both trays during night. For the period between 05:30 and 08:30, the temperature in the tray-1 (T_{c1}) is higher than the temperature in the tray-2 (T_{c2}). That is obvious, because the hot air passes first through the tray-1 than tray-2. However, after 08:30, T_{c2} became higher than T_{c1} . To explain that, it is necessary to analyze the dynamic and thermal behavior in the drying chamber.

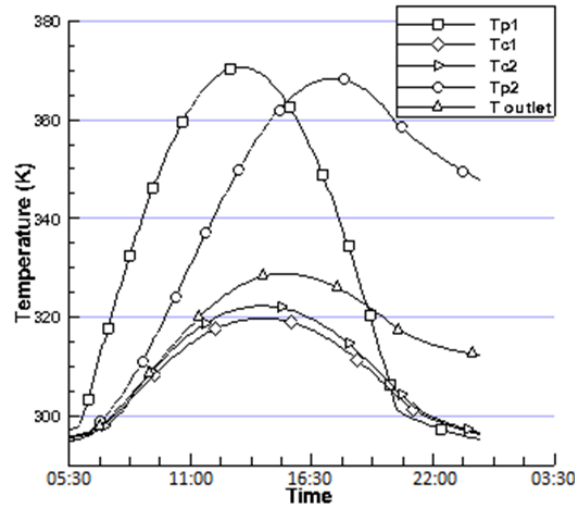


Figure 4

To understand the dynamic and thermal behavior of the airflow within the dryer, temperature and stream function profiles for various hours are presented in Fig. 5. The solar radiation and ambient temperature strongly affects the temperature and airflow behavior inside the solar dryer. The evolution of airflow and temperature of the system follows the variations of those parameters.

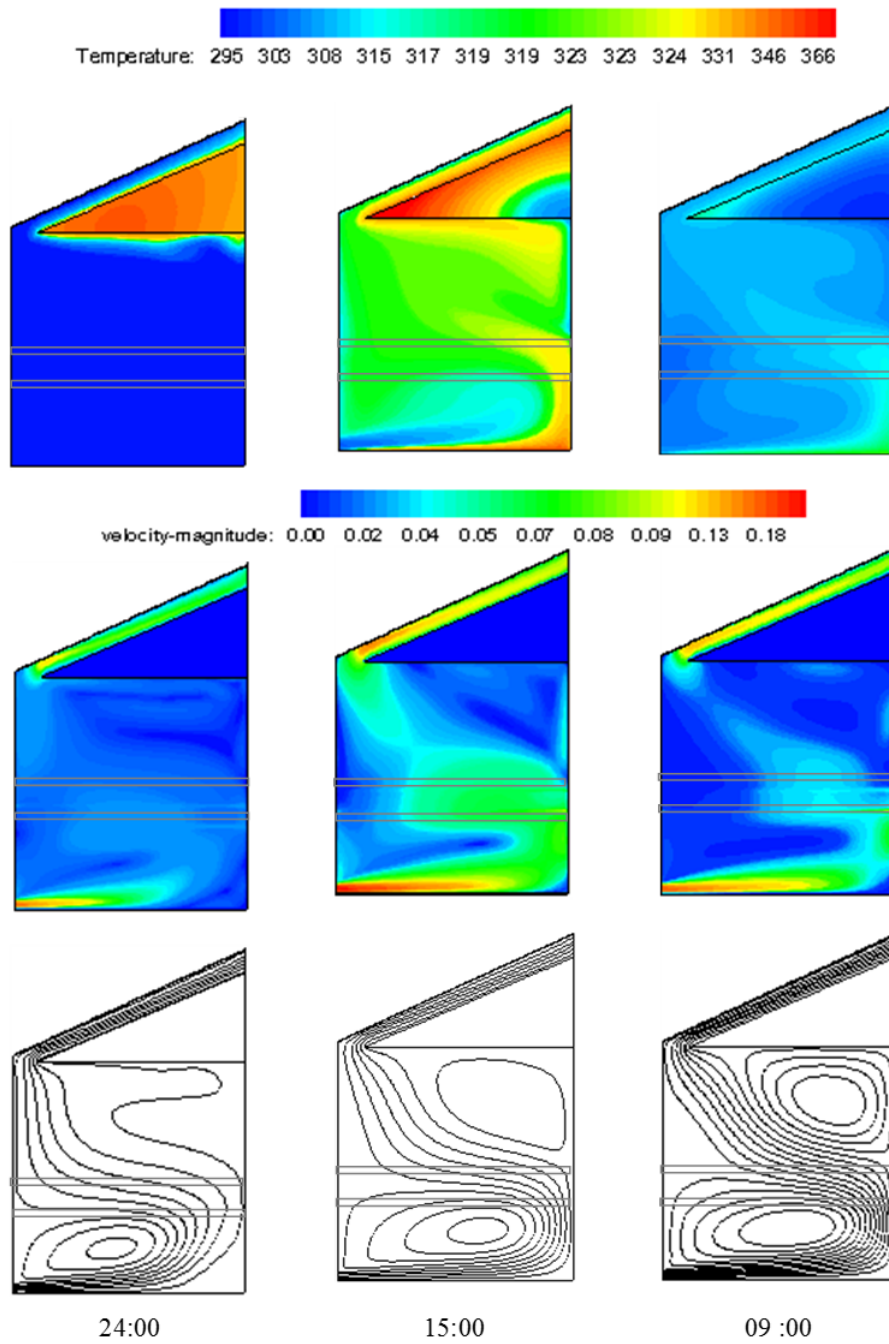


Figure 5

During the solar radiation such as at 09:00, the outside air enters by the bottom to the solar dryer at about 0.14 m/s and flows directly to the wall in front. After heating with the absorber-1, air flows up and goes through the crop trays with reduced velocity. It is observed that the flow in the chamber is divided into two parts; a part passed through the crops trays and flowed outwardly through the solar chimney, the other part returned and generated a vortex with a stagnation point at the lower part of the dryer. Another vortex is generated at the right above corner of the chamber. It favors a convection heat transfer from the granite to the chamber, this behavior clearly appeared at 15:00 and 24:00. Thus T_{c2} is higher than T_{c1} because it received heat from two sources, the heated air coming from the tray-1 and the granite. The average temperature in the drying chamber reached 308 K at 09:00. The plots of the velocity field showed a maximum speed in the vicinity of two absorbers, at the inlet and the outlet of the drying chamber. It achieved 0.20 m/s At 15:00.

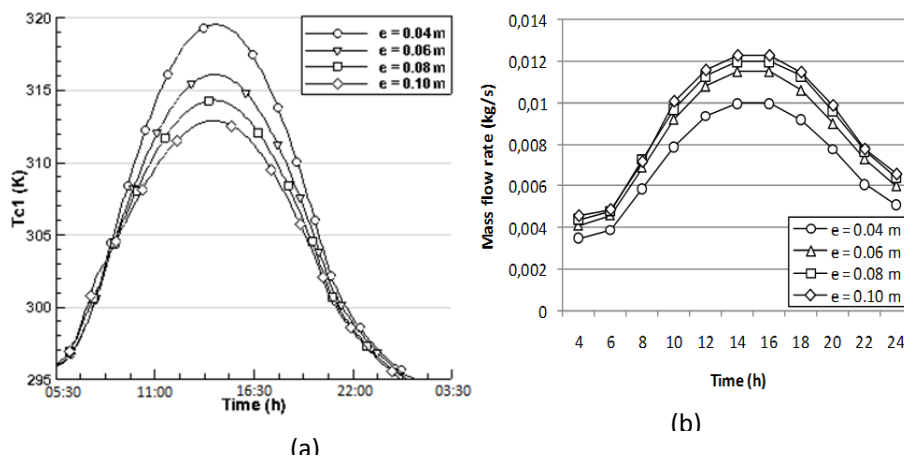


Figure 6

During the night, the temperature of the absorber-1 decreased and the convective heat exchange between the absorber-1 and the airflow became lower, which leads to decrease the average temperature in the drying cabinet to 298 K at midnight. This temperature is weak to ensure drying during nighttime. At the same instant, the temperature of the granite is relatively high, which ensures an extended operation of the chimney even there is no sun because of the heat stored during the day.

4.2.2. Effect of the inlet size on the crops temperature

The evolution of the crops temperature in tray-1 with time for four inlet sizes (0.04, 0.06, 0.08 and 0.10 m) are showed in Fig. 6a. In general, crops temperature increased initially until reached the maximum at noon and decreased after that.

In contrast, it is clear that the maximum crops temperature achieved varies with the inlet sizes. The maximum crops temperature is 320, 316, 314 and 313 K for 0.04, 0.06, 0.08 and 0.10 m, respectively. Thus, the increase in the inlet size from 0.04 m to 0.10 m leads to decrease the maximum crops temperature by about 14%. However, this decrease in temperature declines by half when increasing the inlet size by a constant step.

Comparing to the maximum outdoor temperature (307 K), the maximum crops temperature in tray-1 has increased by 38 %, 26%, 20% and 17% for 0.04, 0.06, 0.08 and 0.10 m, respectively.

To understand the temperature behavior of crops with inlet size, it is necessary to present the airflow rate within the solar dryer for the four sizes (Fig. 6b). Comparison of the airflow rate at different inlet sizes shows that there is a proportional relation between flow rate and size inlet. Increasing the inlet size causes increasing of the airflow rate. Maximum flow rate of about 0.01 kg/s is achieved at 15:00 for inlet size of 0.04 m. This value became 0.0115, 0.012 and 0.0123 kg/s for inlet size of 0.06, 0.08 and 0.10 m, respectively. Thus, the increase in the inlet size by 0.02 m ensures a better extraction of air through the chimney and the flow rate increases by 13, 4.16 and 2.4% by passing from 0.04 to 0.10 m. However, this effect diminishes with the progressive increase of the inlet. The decrease in temperature with increasing the inlet size noticed in Fig. 6a is explained by increasing air flow. When the mass flow rate increased, the air had less time to get hot through the absorber-1. The inlet size of the dryer appears to be a determining parameter to control the process of drying (flow rate and crops temperature). To get a maximum crops temperature with a minimum of input airflow, an inlet thickness of 0.04 m would be more appropriate.

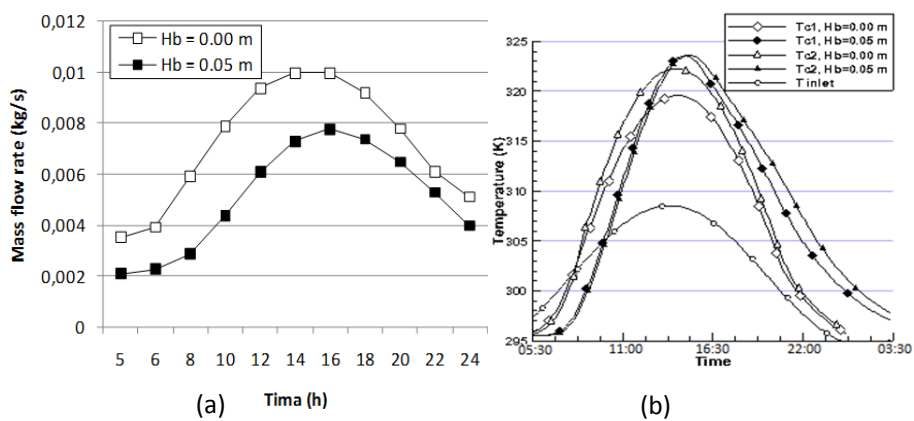


Figure 7

4.3. Solar dryer with a packed bed

4.3.1. Effect of presence of packed bed

In this part, the effect of the presence of a packed bed on the behavior of the system is analyzed. Fig. 7a shows the rate of air circulating over time within the solar dryer without and with packed bed. A small thickness (0.05 m) of gravel was tested for the packed bed. For the two cases the mass flow rate increases over time during the first half day, and slows down drastically afternoon. However, the use of packed bed causes an overall decrease of the mass flow rate over the day, which reached a maximum of 0.0075 kg/s at around 16:00. Without packed bed, a maximum mass flow rate reaches 0.010 kg/s at around 15:00. After, the mass flow rate decreases to 0.005 and 0.004 kg/s during the night (24:00) without and with packed bed, respectively. Thus, using a packed bed with a thickness of 0.05 m can reduce the mass flow rate of circulated air in the chamber between 25% (15:00) and 20% (24:00).

Fig. 7b shows the evolution of the crops temperature on tray-1 and 2 and the inlet temperature without and with packed bed. During the first half day, the crops temperature of the two trays for the both cases increases due to the increasing incident solar radiations. However, crops temperature with the packed bed is lower than without one. The heated air passing through the bed warms up the gravel and the air temperature comes down. Without packed bed, T_{c1} and T_{c2} reached a maximum of 320 K and 319 K at 14:30, respectively. With packed bed, these temperatures reached a same maximum of 324 K at 15 h. Thus, the packed bed reduced the temperature difference between the two trays and improves the drying process by increasing the crops temperature in the both trays. This phenomenon is caused by the presence of the packed bed that decreased the mass flow. After 18:00, solar radiation disappeared and the outside air temperature decreased leading to the decreasing of the crops temperature. The heat stored in the packed bed allowed warming up the circulated air and the crops temperature became higher than without packed bed.

According to Benkhelfellah R. et al. [30] the minimum operational temperature of the solar dryers is about 308 K. Without packed bed, the solar dryer provided temperature higher than 308 K over a period of 10.08 hours. Using a packed bed, this period is extended to 10.41 hours making a gain of 3.24% in term of operating time.

4.3.2. Effect of thickness of packed bed on the crops temperature

To produce a high quality and cost effective product the drying time must be as short as possible without using excessive heat that causes product degradation. In order to optimize the dimension of the packed bed, a comparison between the crops temperature evolution for four thicknesses of the packed bed ($H_b = 0.05, 0.10, 0.15$ and 0.17 m) is presented in Fig. 8. By using a packed bed with a thickness of 0.05 m, the temperature of the crops achieves the maximum of 324 K during the solar radiation and strongly reduces to 296 K at 03:30. One sees also that, during the solar radiation, the maximum crops temperature decreases with increasing the thickness of packed bed. After these hours, the minimum crops temperature increases with the increase of the packed bed thickness. Indeed, a high thickness bed provides

a high thermal storage causing a decrease of the fluctuations of temperature. For a thickness of 0.05, 0.10, 0.15 and 0.17 m the crops temperature achieve around 324, 322, 319 and 317.5 K as maximum and reduce during the night to 297, 301, 305 and 306 K at 03:30, respectively. Comparing to the minimum drying temperature (308 K), the maximum crops temperature is higher by 45%, 40%, 31% and 27% for the previous thickness of packed bed. Increasing a packed bed thickness by 0.05 m can reduce a maximum temperature reached between 3.2% and 6.12%, and increase a minimum temperature reached between 3% and 12%. The low percentage is observed when increasing the thickness beyond 0.15 m. A higher value of packed bed promotes better heat storage and low peak temperature variation. However, this behavior becomes less sensitive beyond a thickness of 0.15 m.

The working period of the solar dryer is extended to 10.41, 11.41, 12.41 and 12.5 hours using thicknesses of 0.05, 0.10, 0.15 and 0.17m, respectively. Therefore a gain of 3.27%, 13.19%, 23.11% and 24% is gotten comparing to the case without packed bed. A thickness of 0.17 m can provide just 2.4 minutes comparing to 0.15 m. In this case a thickness of 0.17 is not recommended.

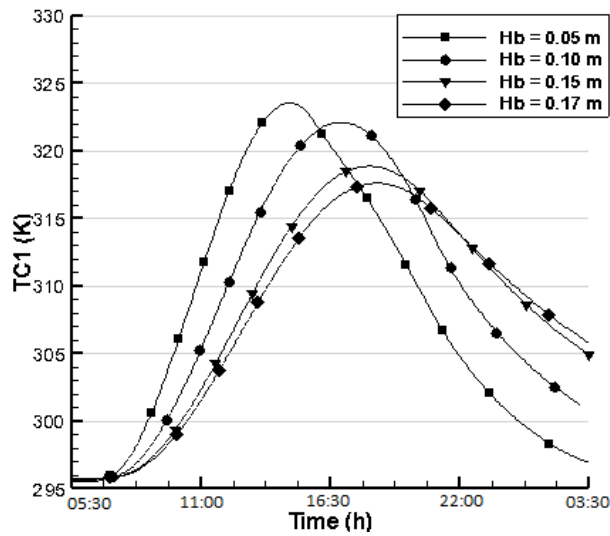


Figure 8

Maximum temperature of drying figs is 323 K, drying them at a higher temperature would result in cooked figs [22]. As precaution, using a thickness of 0.05m is not good because the maximum crops temperature in this case is higher than 323 K. A thickness between 0.10 m and 0.15 m can provide the suitable temperature of drying figs, because it provided a good temperature and good storage in the same time. For this solar drying study, a thickness of 0.15 m could be taken as appropriate because it assures a longer working period.

4.4. Moisture content

The effect of the moisture on the temperature variation is assumed to be negligible in most cases [17, 22]. The moisture content is then computed from equation (17) by using the crops temperature calculated in previous CFD study. For drying process of figs, the average initial moisture content is approximately 1.9 kg of water/ Kg of dry solids (M_0) [24].

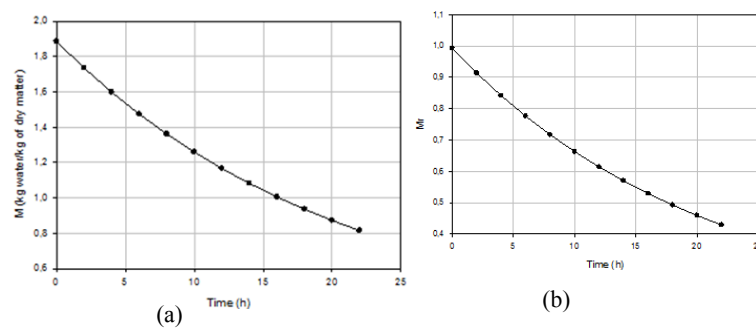


Figure 9

Fig. 9. represents both of variation of moisture ratio (MR) and moisture content in the figs versus time (the 0 represents time at 06:00) in the case of packed bed of 0.15 m. It can be seen that the moisture ratio decreases over the time, that is obvious because the moisture content decrease also over time, this is due to the increasing of crops temperature at the first stage (warming-up period) of drying. During the night hours, the drying process occurred because the packed bed released the heat stored. The moisture content decreased in this case from 1.9 ($MR = 1$) to 0.76 kg water/kg dry solids ($MR = 0.4$) for 22 hours.

5. Conclusion

A numerical study is proposed to simulate airflow and temperature in the solar dryer. Unsteady turbulent airflow and heat transfer through a two-dimensional model was carried out for a typical day of August under the climatic conditions of Tlemcen (Algeria). As a thermal storage, a porous media was integrated in the solar dryer and granite in solar chimney to provide the extraction of air during off sunshine hours. Comparing to the global method used by Jain D. [20], the use of the CFD gives us more details on the flow behavior. The path of the flow, the hot and the cold regions, it helps us to have local informations about the flow parameters (velocities, temperatures, mass flow rate, ect.)

Following specific conclusions are drawn:

1. The maximum velocity and temperature are at the vicinity of the two absorbers.

2. Increasing the inlet size accelerates the extraction of air through the chimney and, the flow rate increases between 13 to 2.4% when gradually increasing the width of the inlet from 0.04 to 0.10 m, respectively. Thus, increasing the air inlet size with a constant step leads to decreasing of the crops temperature by half percent. Therefore, the mass flow rate should be lower using an inlet of 0.04 m.
3. Using only the granite as a thermal storage provide air circulation until 24:00. At this time, the air temperature in the chamber is small to ensure drying, it is necessary to include a packed bed with a suitable thickness inside the drying chamber.
4. The packed bed reduces the temperature difference between the two trays and improves the drying process by increasing the crops temperature in the both trays.
5. Using a packed bed with a thickness of 0.05 m can reduces the mass flow rate extracted around 22%. Increasing a packed bed thickness by 0.05 m improves heat storage and can reduce the fluctuations of absolute temperature between 0.3 and 1.3%. However, this behavior becomes less sensitive from a thickness of 0.15 m.
6. Using a packed bed with a thickness of 0.15 m ensure a better storage. However, the necessary thermal storage for the air circulation, ensured by the granite, is higher than that stored by the packed bed and needed for drying figs. Thus, ensuring a harmonious operation with the both thermal storage is so difficult. Analyzing the mass of granite used in the chimney is therefore necessary for a future study.
7. Using a packed bed of 0.15 m, the moisture content decreased from 1.9 (MR = 1) to 0.76 kg water/kg dry solids (MR = 0.4) for 22 hours.

References

- [1] Sodha, M. S., Bansal, N. K., Kumar, A., Bansal, P. K., Malik, M. A. S.: Solar Crop Drying, *CRC Press: New York, U.S.A.*, **1987**.
- [2] Bala, B. K., Woods, J. L.: Simulation of indirect natural convection solar drying of rough rice, *Solar Energy*, 531, 259–266, **1994**.
- [3] Purohit, P., Kumar, A., Kandpal, T. C.: Solar drying vs. open sun drying: a framework for financial evaluation, *Solar Energy*, 80, 1568–79, **2006**.
- [4] Sharma, A., Chen, C. R., Lan, N. V.: Solar energy drying systems: a review, *Renew Sustain Energy Review*, 13, 1185–1210, **2009**.
- [5] Korti, A. N.: Numerical 3D heat flow simulations on double-pass solar collector with and without porous media, *Journal of Thermal Engineering*, 1, 10–23, **2015**.
- [6] Korti, A. N., Tlemsani, F. Z.: Experimental investigation of latent heat storage in a coil in PCM storage unit, *Journal of Energy Storage*, doi:10.1016/j.est.2015.12.010, In Press, **2015**.
- [7] Lalit, M. B., Santosh, S., Naik, S. N.: Solar dryer with thermal energy storage systems for drying agricultural food products: A review, *Renewable and Sustainable Energy Reviews*, 14, 2298–2314, **2010**.

- [8] **Jain, D., Rajeev, K.:** Performance evaluation of an inclined multi-pass solar air heater with in-built thermal storage on deep-bed drying application, *Journal of Food Engineering*, 65, 497–509, **2004**.
- [9] **Jain, D.:** Modeling the system performance of multi-tray crop drying using an inclined multi-pass solar air heater with in-built thermal storage, *Journal of Food Engineering*, 71, 44–54, **2005**.
- [10] **Berroug, F., Lakhel, E. K., El Omari, M., Faraji, M., El Qarnia, H.:** Thermal performance of a greenhouse with a phase change material north wall, *Energy and Buildings*, 43, 3027–3035, **2011**.
- [11] **Mathioulakis, E., Karathanos, V. T., Belessiotis, V. G.:** Simulation of Air Movement in a Dryer by Computational Fluid Dynamics: Application for the Drying of Fruits, *Journal of Food Engineering*, 36, 183–200, **1998**.
- [12] **Mirade, P.S.:** Prediction of the air velocity field in modern meat dryers using unsteady computational fluid dynamics CFD models, *Journal of Food Engineering*, 60, 41–48, **2003**.
- [13] **Margaris, D. P., Ghiaus, A. G.:** Dried product quality improvement by air flow manipulation in tray dryers, 75, 542–550, **2006**.
- [14] **Wei, C., Man, Q.:** Analysis of the heat transfer and airflow in solar chimney drying system with porous absorber, *Renewable Energy*, 63, 511–518, **2014**.
- [15] **Romero, V. M., Cerezo, E., Garcia, M. I., Sanchez, M. H.:** Simulation and validation of vanilla drying process in an indirect solar dryer prototype using CFD Fluent program, *Energy Procedia*, 57, 1651–1658, **2014**.
- [16] **Ghaffari, A., Mehdi, R.:** Modeling and Improving the Performance of Cabinet Solar Dryer Using Computational Fluid Dynamics, *Int. J. Food Eng.*, 11, 157–172, **2015**.
- [17] **Amanlou, Y., Zomorodian, A.:** Applying CFD for designing a new fruit cabinet dryer, *Food Engineering*, 101, 8–15, **2010**.
- [18] **Suhaimi, M., Sohif, M., Kamaruzzaman, M. H. R., Elias S.:** Comparison of CFD Simulation on Tray Dryer System Between Porous and Solid Product, 7 *WSEAS International Conference on Renewable Energy Sources RES'*, 13, 59–64, **2013**.
- [19] **Goyal, R. K., Tiwari, G. N.:** Parametric study of a reverse flat plate absorber cabinet dryer, *A New Concept Solar Energy*, 60, I, 41–48, **1997**.
- [20] **Jain, D.:** Modeling the performance of the reversed absorber with packed bed thermal storage natural convection solar crop dryer, *Journal of Food Engineering*, 78, 637–647, **2007**.
- [21] **Asan, H., Sancaraktar, Y. S.:** Effect of wall's thermophysical properties on time lag and decrement factor, *Energy and Building*, 28, 159–166, **1998**.
- [22] **Trivittayasil, V., Tanaka, F., Hamanaka, D., Uchino, T.:** Prediction of surface temperature of figs during infrared heating and its effect on the quality, *Biosystems Engineering*, 122, 16–22, **2014**.
- [23] **Norton, T., Sun, D.:** Computational fluid dynamics CFD – an effective and efficient design and analysis tool for the food industry: A review, *Trends in Food Science & Technology*, 17, 600–620, **2006**.
- [24] **Babalís, S. J., Papanicolaou, E., Kyriakis, N., Belessiotis, V. G.:** Evaluation of thin-layer drying models for describing drying kinetics of figs *Ficus carica*, *Food Engineering*, 75, 205–214, **2006**.
- [25] **Kiranoudis, C. T., Maroulis, Z. B., Tsami, E., Marinou-Kouris, D.:** Equilibrium moisture content and heat of desorption of some vegetables, *Journal of Food Engineering*, 20, 1, 55–74, **1993**.

- [26] **Capderou, M.:** Atlas solaire de l'Algerie, tome 2: Aspect énergétique, Edition n°2075.
- [27] **Watmuff, J. H., Charters, W. W. S., Proctor, D.:** Solar and wind induced external coefficients for solar collectors, *CooperationMediterraneenne pour l'Energie Solaire COMPLES*, Revue Internationale d'Héliotechnique, 2nd Quarter, 56. **1977**.
- [28] **Swinbank, W. C.:** Long-wave radiation from clear skies, *Quarterly Journal of the Royal Meteorological Society*, 9, 339–348, **1963**.
- [29] **Jyotirmay, M., Sanjay, M. A.:** Summer performance of inclined roof solar chimney for natural ventilation, *Energy and Buildings*, 38, 1156–1163, **2006**.
- [30] **Benkhelfellah, R., El Mokretar, S., Miri, R., Belhamel, M., :** Séchoirs solaires. Etudes comparative de la cinétique de séchage des produits agroalimentaires dans des modèle de types direct et indirect, *12ième journée mondiale thermique Maroc*, **2005**.
- [31] Météo Tlemcen Zenata: [https://www.meteoblue.com/fr/meteo/prevision/semaine/tlemcen%20zenata _alg%C3%A9rie.6296381](https://www.meteoblue.com/fr/meteo/prevision/semaine/tlemcen%20zenata_alg%C3%A9rie.6296381)

Nomenclature

Latin letters

A_t	mirror surface, m^2
a_w	water activity
C	inertial resistance factor
C'_0	empirical coefficients of Eq.13
C'_1	empirical coefficients of Eq.13
C_1	constant for the turbulence model
C_2	constant for the turbulence model
C'	coefficient of Eq.17
C	specific heat at constant pressure, $J\ kg^{-1}K^{-1}$
c_μ	constant for the turbulence model
D_p	particle diameter
D	air outlet, m
e	air inlet, m
G_{sun}	solar irradiations, Wm^{-2}
G_k	turbulence model coefficient
G	Gravitationnal acceleration, ms^{-2}
Hu	absolute humidity, kg vapor/kg of dry air
h_0	convective heat transfer coefficient due to wind, $Wm^{-2}K^{-1}$
H_b	height of packed bed, m
K	thermal conductivity, $Wm^{-1}K^{-1}$
k'	coefficient of Eq.17
k_d	drying constant, s^{-1}
K	turbulence kinetic energy
M	moisture content of grain, kg water/kg of dry matter
M_e	equilibrium moisture content, kg water/kg of dry matter
M_0	initial moisture content of crop, kg water/kg of dry matter
N	normal coordinate, m
P	pression, Pa
Pa	atmospheric pressure, Pa
Pr	Prandtl number
R	universal gas constant, $J\ K^{-1}\ mo^{-1}$
S	source term
T	temperature, $^{\circ}C$ or K

v_j	velocity magnitude y direction, $m.s^{-1}$
v_a	air velocity, $m.s^{-1}$
V_v	wind velocity; m/s
x	horizontal coordinate, m
Y	vertical coordinate, m
Greek symbols	
A	coefficient of absorbtion
B	coefficient of thermal expansion
ε	dissipation rate of turbulence energy (m^2s)
T	transmitivity of glass cover
ρ	density, kgm^{-3}
ρ'	coefficient of reflectivity of mirrors
μ_t	turbulent dynamic viscosity, $kg\ (m\ s)^{-1}$
M	dynamic viscosity, $kg\ (m\ s)^{-1}$
σ	radiation coefficient
σ_t	constant for the turbulence model
σ_k	constant for the turbulence model
σ_ε	constant for the turbulence model
ϵ	porosity
θ	coefficient of permeability
τ	coefficient of transmissivity

Subscripts

A	ambient
a_1	absorber-1
a_2	absorber-2
c_2	crops in tray-2
Eff	Effective
f	fluid phase in packed bed
G	glass cover
m	average
ref	reference
s	solid phase in packed bed
w	wood